Sensors and Actuators A 295 (2019) 177–187

Contents lists available at ScienceDirect

Sensors and Actuators A: Physical

journal homepage: www.elsevier.com/locate/sna

Microfluidic contact lenses for unpowered, continuous and non-invasive intraocular pressure monitoring

Hongbin An [a], Liangzhou Chen [a,*], Xiaojun Liu [a], Bin Zhao [a], Hong Zhang [b], Zhigang Wu [a,c]

[a] School of Mechanical Science and Engineering, Huazhong University of Science and Technology (HUST), Wuhan 430074, China
[b] Department of Ophthalmology, Tongji Hospital, Tongji Medical college of HUST, Wuhan 430074, China
[c] Department of Engineering Sciences, The Angstrom Laboratory, Uppsala University, Uppsala 75121, Sweden

ARTICLE INFO

Article history:
Received 9 November 2018
Received in revised form 6 January 2019
Accepted 29 April 2019
Available online 1 June 2019

Keywords:
Intraocular pressure
Microfluidic contact lenses
Non-invasive
Unpowered
Sensing mechanism

ABSTRACT

Intraocular pressure (IOP) is a crucial physiological indicator of the visual system and play a key role in the diagnosis and treatment of glaucoma. However, the current handheld single measurement tools for IOP sensing cannot meet the future demands for glaucoma management. Thus, here we present the microfluidic contact lens sensors that could provide unpowered, continuous and non-invasive IOP monitoring. The microfluidic contact lens is comprised of a sensing layer of the micropatterned soft-elastomer and a hard plastic reference layer. The devices use the annular sensing chamber filled with the dyed liquid and a sensing microchannel as the IOP transducer. Resulting from the volume variance of the sensing chamber and caused by the deformation of the sensing layer under pressure, the IOP signal is detected as the displacement change of the dyed liquid's interface in the sensing channel, and in which, the displacement change can be optically observed by using the smart-phone camera. Based on the silicone rubber model eyeball, the sensing mechanism of the devices with different design parameters (the position of the sensing chambers and the dimension of the sensing channels) are explored by using the theoretical analyses and experimental investigations. The characteristics of these microfluidic contact lens sensors are tested, in which, the maximum sensitivity of the device (with the sensing chamber of 8.5 mm in diameter and the sensing channel of 100 × 40 um in size) can be achieved to 0.708 mm/mmHg in a working range of 0~40 mmHg. Also, cyclical tests were conducted and indicated that the devices had a good reversibility and Long-term stability. Furthermore, the device (with the sensing chamber of 5.0 mm in diameter and the sensing channel of 150 × 40 um in size) was test on the porcine eyes *ex vivo*, showing a sensitivity of 0.2832 mm/mmHg in a range of 8~32 mmHg and, the device had a good reproducibility to its IOP change. This work provides a promising approach for unpowered, continuous and non-invasive monitoring of IOP.

1. Introduction

Intraocular pressure (IOP) is a crucial physiological indicator of the visual system [1]. Studies have shown that pathological increase in IOP is the main cause of glaucoma [1–5], which is one of the three leading causes of blindness in humans and affects 67 million people worldwide now [5,6]. This is mainly because exorbitant IOP would pinch the optic nerve and cause the visual impairment [1,7]. Studies show that, because of a lack of awareness of vision loss, glaucoma patients may have lost at least 50% of their vision irreversibly before their disease being diagnosed [8,9]. Thus, accurate screening of IOP is the key for the diagnosis of glaucoma [1,9]. Currently, IOP screening was performed by measuring the IOP regularly over a day or period of time with a handheld single measurement tonometer [10], such as Goldman applanation tonometry (GAT) [11], to determine if IOP is too high. Its measuring results were accurate and reliable. However, the patients need to be anaesthetized and professional doctors are needed to operate the tonometer regularly and uninterruptedly during the process, these make the measuring complex, inconvenient and tiring. Thus, continuous and automatic monitoring of IOP is of great significance [12].

Based on the need, some new technologies have been studied for continuous IOP monitoring, including the ocular implantable devices and smart contact lens. The implantable devices for IOP

* Corresponding author.
E-mail address: chenlz@hust.edu.cn (L. Chen).

https://doi.org/10.1016/j.sna.2019.04.050
0924-4247/

sensing, such as LC wireless sensor [13–18], microfluidic devices [19] and optical implant [20], can measure the IOP directly, wirelessly and continuously. However, the sensor implantation process is invasive and requires surgery, causing it unacceptable for most people. Smart contact lenses as minimally invasive wearable platform for ophthalmological diagnostics and treatments have been widely studied in recent years [21,22], including the tear glucose monitoring [23–26], assistant management of the colour vision deficiency (colour blindness) [27], drug dispensing for ocular disease treatment [28] and IOP sensing for glaucoma diagnosis [29–35]. As one of them, smart contact lens (SCL) for IOP sensing are the devices embedded sensing elements on the soft contact lens [21,29–35], it is non-invasive and can be wore on the cornea to detect the IOP from the curvature change of the cornea [29]. As the IOP increase, the inflating cornea will drive the attached soft contact lens to deform conformally, causing the inside sensing elements deform and then lead to the changes in their electrical properties. Some sensing elements with different working principles have been integrated inside the lens, such as strain gauge [29–32], capacitor [33,34] and inductance [35]. Also, some different wireless transmission technologies are applied on the devices, such as the LC resonant wireless techniques [34,30–35] and RFID techniques [22–24,30]. While these mechanoelectrical devices show a good prospect, its further developments are still restricted, because of the potential health-issues of the powered RF electromagnetic radiation to the human body and that, the low air permeability of the electrical components and the mechanical mismatch of the sensing elements with the cornea may cause discomfort to the human eyeball [31].

Lately, as a branch of wearable microfluidics [36–38], microfluidic contact lenses [39] have been proposed and showed a promising prospect in diagnosis and treatment of ophthalmic, especially in tear component analysis and controlled drug release for ocular disease treatment. While, as for IOP measurement, John Yan [40] had presented the contact lens integrated with microfluidic pressure sensor to detect the curvature change of the cornea. Similar to the existing wearable microfluidic devices for biophysical sensing (e.g. tactile sensing [41–44], strain sensor [45,46] and pulse pressure sensing [47]), it intends to achieve the IOP continuous measuring based on the principle of liquid manipulation [36]. Because the IOP measuring is carried out by using a camera to identify the displacement of the dyed liquid in the sensing channel, this passive visual measurement method would not produce RF electromagnetic radiation and is considered harmless. Nevertheless, the devices they prepared were only tested on a plane force gage and had not realized the IOP measuring on the curved surface, which means that, the IOP sensing mechanism of microfluidic contact lenses has not been studied. Well, in our previous study [48], we presented a useful and robust approach to make wearable microfluidic lenses via a combination of irreversible bonding and thermoforming technology. We used plastic—PET (polyethylene terephthalate) and the silicone rubber—PDMS (polydimethylsiloxane) to prepare the contact lens, and integrated the PDMS material in the inner side of contact lens, to contact with the cornea. Since PDMS is soft, biocompatible, highly oxygen-permeable, and it can be easily modified hydrophilic [36], it makes the contact lens comfortable to wear and allows the devices to detect the cornea deformation varied with pressure. In addition, in our previous study [48], the device was proved to be pressure-sensitive under the plane force. Thus here, based on the need, we employ it to realize the unpowered, continuous and non-invasive monitoring of IOP on curved surface.

In this study, we explore the mechanism for sensing IOP on curved surface by using the microfluidic contact lens sensors with different design parameters. The designs, simulations and performances of these microfluidic contact lenses for IOP sensing are presented.

2. Experiments

2.1. Device working principle

Fig. 1(a) show the actual fabricated microfluidic contact lenses with different design parameters. Fig. 1(b) illustrate the cross-section of a microfluidic contact lens wearing fitted on the eyeball. The microfluidic contact lenses comprise of a sensing layer of the micropatterned PDMS and a hard PET reference layer, to form the sensing chamber, sensing channels and the buffer chamber. In which, the sensing chamber is filled with the dyed liquid and works to feel the cornea deform. The long sensing channel is partly filled with the red liquid and works to accommodate the spare dyed glycerol which flows from the chamber. While, the out-flow chamber is empty and its volume is designed much larger than the liquid volume to prevent dye leakage. The IOP sensing principle of microfluidic contact lens is similar with a micropump system. As shown in Fig. 1(b) and (c), when the IOP is applied on the eyeball wall and increases, the cornea follows to deform, leading to the sensing chamber being compressed. The volume of the sensing chamber decreases, while the total volume of the liquid remains the same during the process. So, the liquid in the compressed chamber flow forward to the sensing channel, creating a displacement change of the liquid interface in the sensing channel. In turn, as the IOP released, the fluid would flow back due to the vacuum force generated from the PDMS recovery. Combining Fig. 1(b)–(d), the displacement of the liquid interface, Δl, and the sensitivity, t, can be calculated as following:

$$\begin{cases} \Delta l \approx \dfrac{-L \cdot \Delta S}{wh} = \dfrac{-L}{wh} \cdot \Delta S \end{cases} \tag{1}$$

$$\begin{cases} t = \dfrac{\Delta l}{\Delta P} \approx \dfrac{-L}{wh} \cdot \dfrac{\Delta S}{\Delta P} \end{cases} \tag{2}$$

$$\begin{cases} \Delta S = S_2 - S_1 \end{cases} \tag{3}$$

$$\begin{cases} L = R\varphi \end{cases} \tag{4}$$

$$\begin{cases} \Delta V = -L \cdot \Delta S \end{cases} \tag{5}$$

Where Δl represents the displacement of red liquid in sensing channel, t is the devices sensitivity; L, R and φ represents the length, radius and angle of the annular distributed chamber; w and h is the width and height of the rectangular sensing channel, respectively; S_1 and S_2 is the sectional area of sensing chamber under pressure of P_0 and P_0+ΔP, so, ΔS represents its variation; ΔV is the volume changes of the chamber. From Eq. (2), by increasing the length of the annular distributed chamber or decreasing the sectional area of sensing channel, the device's sensitivity can be increased. Obviously, by using smart phone to optically detect the fluidic displacement in sensing channel, the resulting IOP can be determined.

2.2. Devices designs and fabrication

As shown in the Table 1, we design and fabricate the microfluidic contact lenses with different dimension parameters (the position of the sensing chambers and the dimension of the sensing channels). These microfluidic contact lenses were all designed and fabricated with the same sizes (with curvature radius of 8.0 mm and diameter of 14.4 mm). However, the microfluidic contact lenses were manufactured by using chemical assisted bonding and next thermoforming technologies, in which, the micropatterned PDMS films and the thermoplastic plastic, PET films, were first irreversibly bonded to form the plane devices and then thermoformed to the spherical. Since the devices were 3D stretched during thermoforming, the width and height of the rectangular sensing chambers

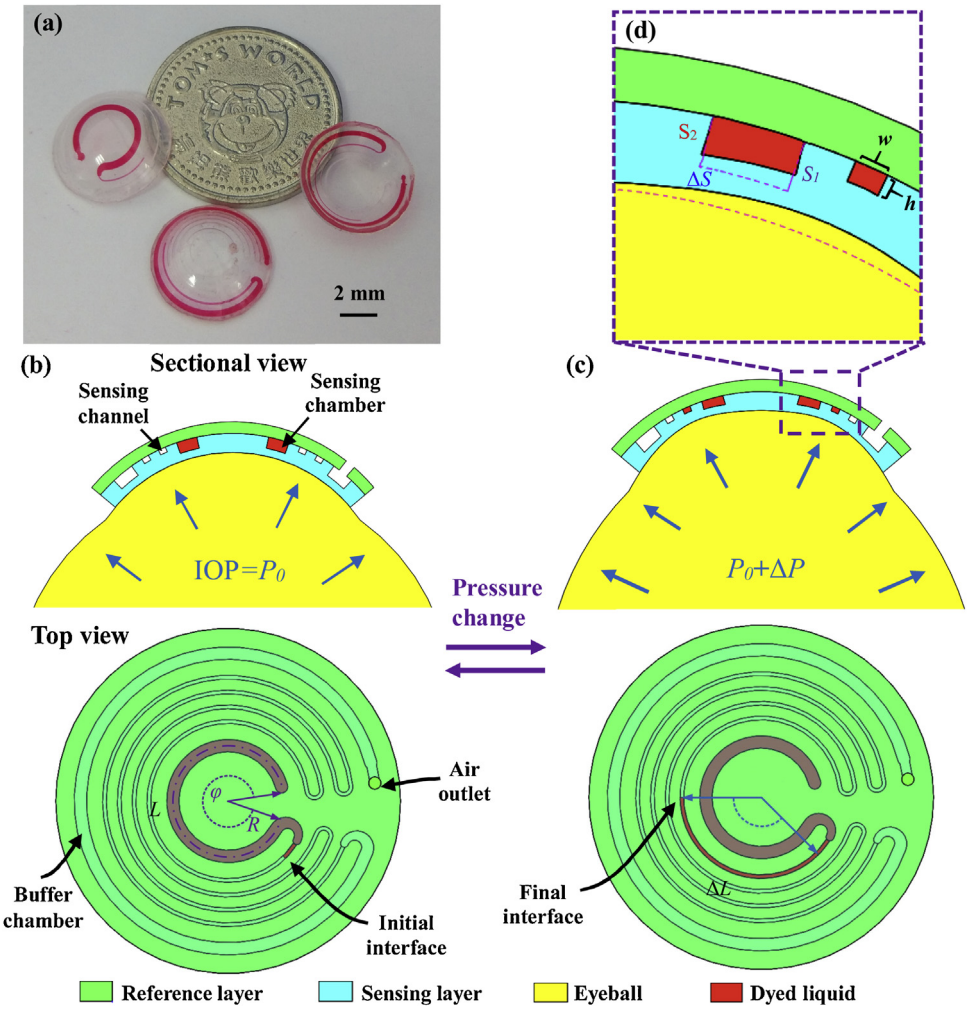

Fig. 1. Schematic illustration of the sensing principle of microfluidic contact lenses for IOP sensing. (a) Actual fabricated microfluidic contact lenses. (b) (c) Sectional view and top view of microfluidic contact lenses under different IOP of P_0 and $P_0+\Delta P$; (d) Picture showed the sectional area change of sensing chamber.

Table 1
The designed dimension parameters and their variation levels.

Parameters	The curvature radius and diameter of lenses (mm)	The expected width and height of chamber on lenses (μm)	*R*: The diameters of the sensing chambers (mm) and its designed width and height on wafer (um)	$w \times h$: The width and height of sensing channels (μm)
levels	8.0 and 14.4	700 × 250	D_1: 5.0 mm; 670 × 255 um D_2: 8.5 mm; 610 × 260 um D_3: 12.0 mm; 485 × 305 um	100 × 40 150 × 40 200 × 60

on contact lens have changed, compared with its original sizes on plane. In our previous study, we have shown that thermoforming does not remarkably affect the channel distributions, and the spherical stamping process was similar to the process of mapping the annular distributed channel from plane to spherical along the central axis. But, the channel distributions showed a significant influence on the channel size; the width and height of the outer distributed channel changed more than the inner. While we design the sensing chambers, with the same width and height of 700 × 250 μm but three different distributed diameters (with D_1 = 5.0 mm, D_2 = 8.5 mm and D_3 = 12.0 mm) on these contact lenses. So according to the width and height's change-rate of different distributed channels after thermoforming, the width and height of these sensing chamber patterns on wafers were designed to be 670 × 255 μm, 610 × 260 μm and 485 × 300 μm respectively. The cross sections of the three chambers after thermoforming were shown in Fig. S1 and their dimensions were measured to close to 700 × 250 um. Also, the angle: φ of the three chambers was designed to be 320°, 330° and 336°respectively. In addition, the multi-circle distributed sensing channel, with total length of 98.8 mm, was designed with three levels of 100 × 40 μm, 150 × 40 μm and 200 × 60 μm, respectively. But since the rectangular sensing channels were very small and, the width of sensing channel increased while the height of it decreased after thermoforming, its cross-sectional area varied little after the process.

Fig. 2 illustrates the fabrication process of these microfluidic contact lenses, the process can be summarized as the following five steps: soft lithography, silanization of the substrate, plasma-treated bonding, thermoforming and liquid injection. For the sensing layer, the micropatterned PDMS (Sylgard 184, MI, USA) was made by using the conventional photolithography and replica molding techniques (soft lithography), Fig. 2(a–c). The replica mold

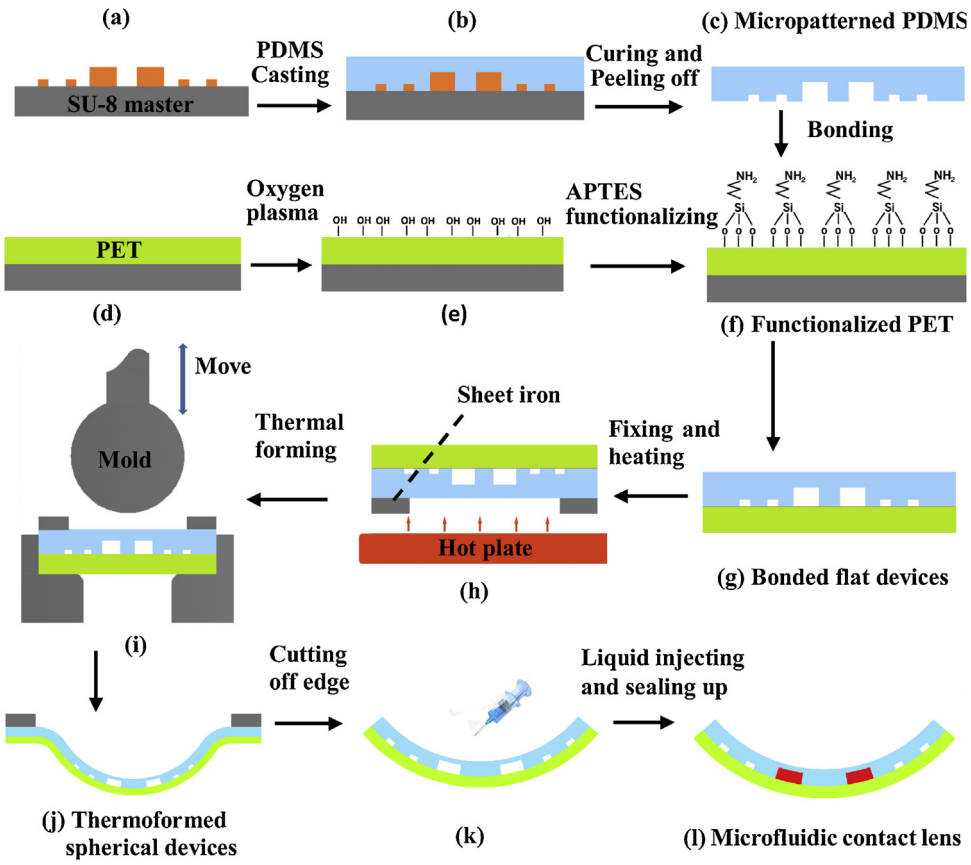

Fig. 2. Schematic illustration of fabricating microfluidic contact lenses. (a–c) The schematic of process flow for manufacturing micropatterned soft-elastomer; (d–f) The schematic of the process flow for PET treatment; (g) The picture of bonded PET-PDMS assembly; (h–j) The schematic illustration of thermoforming progress to press the plate into the spherical cap; (k–l) The schematic illustration of liquid injecting.

consisted of a two-step SU-8 (Microchem, Inc.) process on the silicon substrate to, make the molding structures of the sensing channels and chambers with different dimension parameters. After making the 3-D mold, the non-curing PDMS (two components mix in a 40:1 ratio and degassed) was poured onto the pattern, and spin-coated at 500 rpm for 11.5 s. After curing at 80 °C for 90 min, the PDMS layer were peeled off from wafer with a thickness of approximately 500 μm and a Young modulus measuring between 0.242 to 0.277 MPa under the small deformation (with six samples separately subjected to the tensile and compression tests by using the international standards, ISO 37: 2005 and ASTM D575-91, to experimentally determine their load–displacement data). The chemical assisted bonding was completed by using silane coupling agent, APTES (99%, Sigma-Aldrich, USA), to form silylation of the surface of PET (silanization of the substrate), Fig. 2(d–f). During the process, the PET membranes (0.2 mm, posted up on wafer) were firstly oxygen-plasma activated, resulting in the hydrophilization of PET surface. The activated PET was then dipped into the prepared solution (5%-concentration ratio; heated at 80 °C) for 20 min to functionalize the surface of PET. Next, the PDMS and the functionalized PET were oxygen-plasma activated to form Si–OH groups on both surfaces. Then, the two members were immediately brought into contact, and bonded, Fig. 2(g). The bonded devices were fixed on a square clip and thermoformed into spherical under the action of terrace die (curvature radius: 8.0 mm) after it was heated at 170 °C for 35 s, Fig. 2(h–j). Following, the edges of the thermoformed devices were trimmed off and the contact lenses were prepared to a diameter of 14.4 mm, Fig. 2(k). After that, a controlled volume (with volume of 2.749 μL, 4.673 μL and 6.596 μL for the three kinds of the thermoformed devices) of red glycerol solutions was infused into the chambers. The red liquid was prepared in a ratio of 4:1:0.1 by mixing the harmless liquid, deionized water and glycerol, to the colour dye (Acid Red G). After sealing up the Injection port, the microfluidic contact lenses were finally manufactured with a thickness of about 650 μm. This thickness is between the commercial silicone lenses, the Silsoft® lens [30] from Bausch & Lomb, NY, USA (with a thickness of up to 710 μm and is approved for an extended wear of 30 days) and the Triggerfish® contact lens sensor [31] (with a thickness of about 585 μm at the center and is approved in clinical trials).

2.3. Finite element modelling

According to Eq. (1), the displacement is directly proportional to the change of the cross-sectional area of the sensing chamber. So, by using finite element modelling (FEM), we explored the influence of different IOP to the cross-sectional area of the sensing chambers with different distributions. The FEM was performed in COSMOL simulations. Based on solid mechanics module, we used the 2-D axisymmetric model to replace the 3-D sphere for simulation. The annular distributed sensing chambers, with same size of 700 × 250 um, were set up with different diameters (D_1 $\tilde{D}_3$ = 5.0, 8.5 and 12.0 mm) for analysis. While, boundary conditions were fixed at the bottom of eyeball, and a pressure with range of 0 to 5.33 K Pa (0 to 40 mmHg) was applied on inner wall of eyeball. Surface integral was used to calculate the cross-sectional area of these chambers.

2.4. Characterization of microfluidic contact lenses for IOP sensing

The contact lenses sensors were tested on the silicone rubber model eyeball to characterize their IOP monitoring performance.

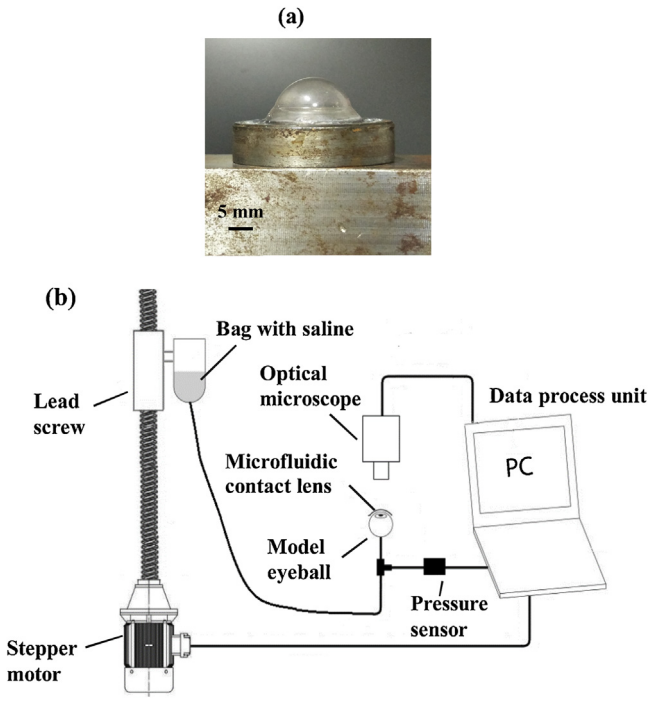

Fig. 3. (a) the actual model eyeball; (b) Schematic illustration of the testing setup for microfluidic contact lenses.

Table 2
Design parameters of the model eyeball.

Radius of curvature (mm)	8.0
Thickness of the rubbery cornea (um)	500
Poisson ratio	0.49
Elastic modulus of the silicone rubber (MPa)	0.85õ.93

Fig. 3(a) shows the actual model eye, while Table 2 shows its design parameters (see the Fig. S2 for its detailed dimension parameters). The model eye was fabricated by using the PDMS material, in which, the PDMS and its curing agent was first mixed in a 15:1 ratio and then cast into the mold (with curvature radius of 8.0 mm). After curing at 80 °C for 90 min, the silicone rubber was peeling off from the mold with a Young modulus measuring between 0.851 to 0.928 MPa (six samples were separately subjected to the tensile and compression tests by using the international standards, ISO 37: 2005 and ASTM D575-91, to determine their load–displacement data under small deform). After that, the spherical PDMS was fixed onto a custom fixture by using an instant strong adhesives and the model eye was finally made up. Fig. 3(b) shows the testing set up to characterize the devices performance. In which, a T-shaped fluidic interconnect was introduced and connected with the fixed model eye and the pressurization device. As for the pressurization device, a bag with saline was drove up and down by the ball bearing lead screw mechanism to load pressure on the model eyeball through the medical catheter. While, a pressure sensor (PX273–300DI, Omega Engineering Inc., USA) was connected with the remaining port of the T-shaped interconnect to independently characterize the loop IOP. An industrial optical microscope (GP-660V, GAOPIN. inc, China), with CCD pixels of 200 million, frame rate of 45 fps @1920×1080, electronic magnification of 14–90 and maximum view field of 52×38 mm, was used to detect the position of liquid in the sensing channel of microfluidic contact lens. Through the upper computer, the signal of pressure sensor and the CCD signal can be received, also, the stepper motor can be controlled to load static or dynamic pressure on the model eyes. The IOP was controlled between 0 mmHg to 40 mmHg in the tests and the tests were conducted in a thermostatic chamber (with temperature of 20 °C).

3. Results and discussion

3.1. FEM result

Fig. 4(a) shows the simulation illustration of three sensing chambers with diameters of 5.0, 8.5 and 12.0 mm (the results obtained by setting the three chambers in one contact lens are the same as the results of setting the three chambers in three contact lenses separately). According to the measured Young's modulus, the sensing layer was modeled as an elastic material, with a compressive modulus setting of 0.25 MPa. Also, the model eye was set as an elastic material, with a modulus of 0.9 MPa. Fig. 4(b) and (c) show the result of the device under 40 mmHg pressure, the stress diagram and displacement diagram. The two inner sensing chambers (with D_1 $\tilde{D}_2$ = 5.0 and 8.5 mm) was found to be squeezed, its cross-sectional area was calculated to be down. So, the liquid in these compressed chambers would flow to the sensing channel under pressure. While, for the out distributed chamber (D_3 = 12.0 mm), it was lateral shifted and stretched, its cross-sectional area was computed to be increased. Thus, theoretically, its experimental phenomenon will be the opposite. When the IOP increases, its liquid would flow out from the sensing channel to the chamber, due to the vacuum force generated from the chamber volume increase. Fig. 4(d) shows the cross-sectional area of the three chambers varied with pressure. The chambers with distributed diameters, D_1 = 5.0 mm and D_2 = 8.5 mm, show the same trend. With the pressure increase, their cross-sectional area down linearly. But, the more inside chamber (D_1 = 5.0 mm) decreases more. The chamber with the outset distributed, D_3 = 12 mm, show a contrary trend. Its area rises (with pressure at 0–32 mmHg) nonlinearly with the increase of pressure, in which, the change rate gradually decreases to zero. For the pressure at 32 to 40 mmHg, the area decreases but the reduction is very small. Fig. 4(e) shows the volume changes ($\Delta V = -L \cdot \Delta S$) of the three chambers varied with pressure, their change trend is as same as that of the cross-section area. However, the sensing chamber of 8.5 mm in diameter shows a bigger change, compared with the chamber of 5.0 mm, this is mainly due to that its length (L) is longer.

3.2. Devices sensitivity

The microfluidic contact lenses were put on the silicone rubber model eye, and fitted well with its surface. Based on the pressurizing system, their static performance were tested. The model eye was pressurized between 0 to 40 mmHg, the displacement changes and the pressure after stabilization were recorded. Fig. 5 shows the experimental output displacement of these microfluidic contact lenses varied with the input pressure. Fig. 5(a) shows the results of the devices, having same distributed chamber of 5.0 mm in diameter but different sensing channel of 100 × 40, 150 × 40 and 200 × 60 μm in dimensions. The sensing responses of the three devices varied linearly with IOP (with R^2 = 0.973, 0.977 and 0.970 respectively). The three devices showed the positive displacement changes and had a sensitivity of 0.607, 0.395 and 0.223 mm/mmHg respectively. The result indicates that, the device sensitivity would increase with the decrease of the sectional area of the sensing channel, since their sensing chambers deform same under same pressure. Fig. 5(b) shows the results of the devices with same distributed chamber of 8.5 mm in diameter but different sensing channel. The sensing responses of the three devices also varied linearly with IOP (with R^2 = 0.976, 0.966 and 0.968 respectively) and showed the positive displacement

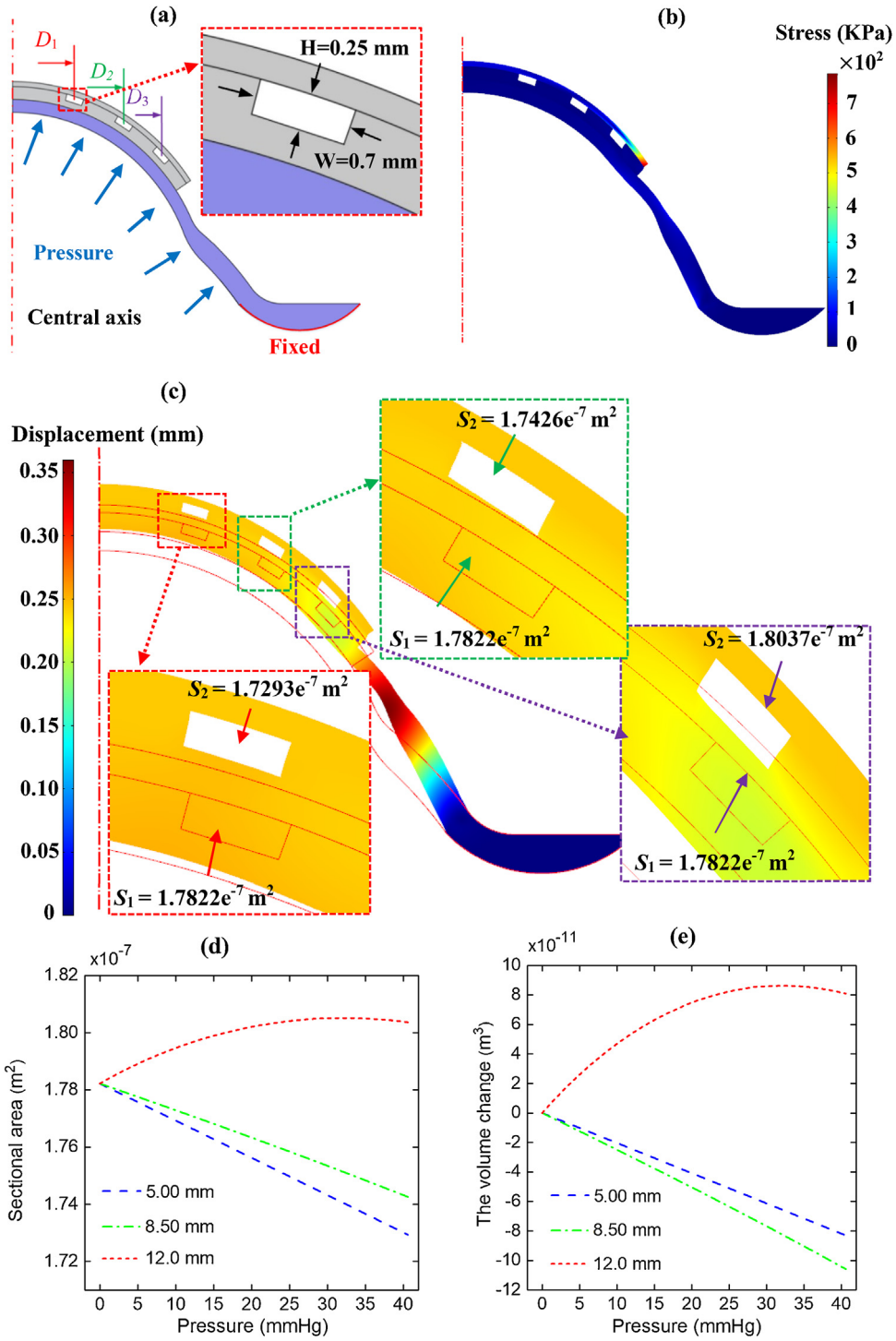

Fig. 4. FEM results of microfluidic contact lens. (a) Simulation illustration; (b) and (c) Sectional view of the sensor with a pressure of 40 mmHg in relation to its stress and deformation respectively; (d) and (e) Comparison of the sectional area and the volume change of the three chambers varied with pressure.

changes. While, the three devices had a higher sensitivity of 0.708, 0.474 and 0.273 mm/mmHg respectively, compared with the inner distributed chamber (D_1 = 5.0 mm). This is consistent with the simulations that its volume change was larger. Besides, the longest distance that the red liquid moves to was found to be 26.1 mm, under IOP of 37.4 mmHg (the device with sensing channel of 100 × 40 μm in dimension), so there is still a long distance to the out-flow chamber. As shown in Fig. 5(c), for the group with outer distributed chamber of 12.0 mm, it showed the same phenomenon in sensitivity, the devices with smaller sensing channel size showed a stronger response. However, the devices showed a negative displacement. When the pressure increased, the liquid flowed from the sensing channel to the sensing chamber; and when the IOP decreased, the liquid flowed back to the sensing channel (see the Movie.S1). This is corresponded to the simulation results that the chamber's sectional area rises with the increase of IOP, causing the liquid move opposite. Also, similar to the change trend of simulation, their response became highly non-linear and saturated under high pressure (27 to 40 mmHg). We use the quadratic polynomial fitting to deal with the non-linear response and it shows

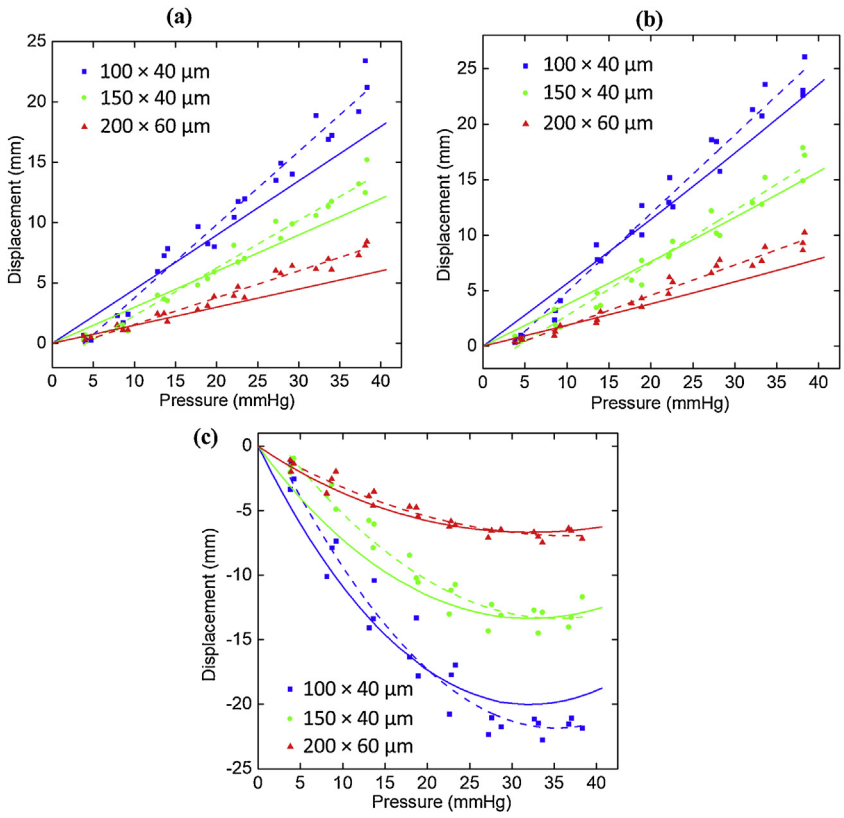

Fig. 5. Experimental investigations on the device sensitivity. (a) For the devices with same distributed sensing chamber of 5.0 mm in diameter but different in dimensions of the sensing channels; (b) For the devices with same distributed sensing chamber of 8.5 mm in diameter; (c) For the devices with same distributed sensing chamber of 12.0 mm in diameter; where the measurement results (dots) with the corresponding fitting curves (dashed lines) are plotted against the theoretical predictions from Eq. (1) (solid lines).

the coefficient of determination with $R^2 = 0.952$, 0.949 and 0.936, respectively. It was also found that the sensitivity of the measurement results with the corresponding fitting curves are higher than that of the theoretical predictions, this might be caused by many factors such as that the central axis of contact lens and the central axis of model eye was not aligned during the test, the sensing channel also deformed during the test or their existed deviation between the mechanical strength of the actual model eye or PDMS sensing layer with that of the simulation setting.

3.3. Device reversibility, response time and long-term stability

Since the sensing responses of the microfluidic contact lenses, with same distributed chamber of 5.0 mm in diameter, were linear; we use them to investigate the reversibility of the sensors under repetitive loads. In which, the model eye was cyclically pressurized by using the slow stair-case stimulus and the quick Max/Min stimulus, the images of the sensors were taken every second to record the displacement changes. Fig. 6(a) shows the results of these devices with different sensing channels of 200 × 60, 150 × 40 and 100 × 40 μm in dimensions, from top to bottom. As for the slow stair-case stimulus, the three devices were able to follow the changes of IOP in time. While, for the quick Max / Min stimulus, it was found that their displacement changes lagged behind the pressure change, especially for the two devices with small sensing channels. Also, compared their dynamic feedback, it can be concluded the tracking characteristics of the devices become better with the dimension of sensing-channel increase. This is mainly due to that the sensing channel become smaller, causing the channel loop resistance increase. In particular, since the human IOP usually change slowly, the sensors can satisfy the use. Overall, the sensor can respond to the cyclic loads within the applied IOP, suggesting a good reversibility (see the Movie.S2).

Since the liquid circuit of the pressurizing system is long, it cannot apply a step signal to the model eye. To determine the time constant of the devices, a force gage connected to a step motor was adapted to apply step pressure to the sensing chamber and the images of the sensors were taken every 0.1 s to record the positions of the liquid interface. Fig. 6(b) show the result, the time constant of the three sensors were 0.33 s, 0.81 s and 1.19 s respectively, the device with large sensing channel shows a lower time constant.

Long-term stability and absence of signal drift are important for IOP sensing, since the contact lens sensor would be wore on the eyes for long time measuring. The long-term stability test was completed by operating the device (with chamber of 5.0 mm in diameter and sensing-channel of 200 × 60 μm in dimensions) in the high IOP (35 mmHg) state or low IOP (10 mmHg) state for long time (1 h) alternately. The test was conducted by increasing the pressure to the high IOP state firstly, and then turned the IOP state. After 3 cycles, the device was turned to the Minimum. Fig. 6(c) shows the long-term testing resulting in a stable displacement for different IOP state, suggesting a good Long-term stability of the device.

3.4. Demonstration of microfluidic contact lens on porcine eyes ex vivo

To demonstrate the adaptability and utility of the microfluidic contact lens sensor on real eyes, we applied the devices to test on

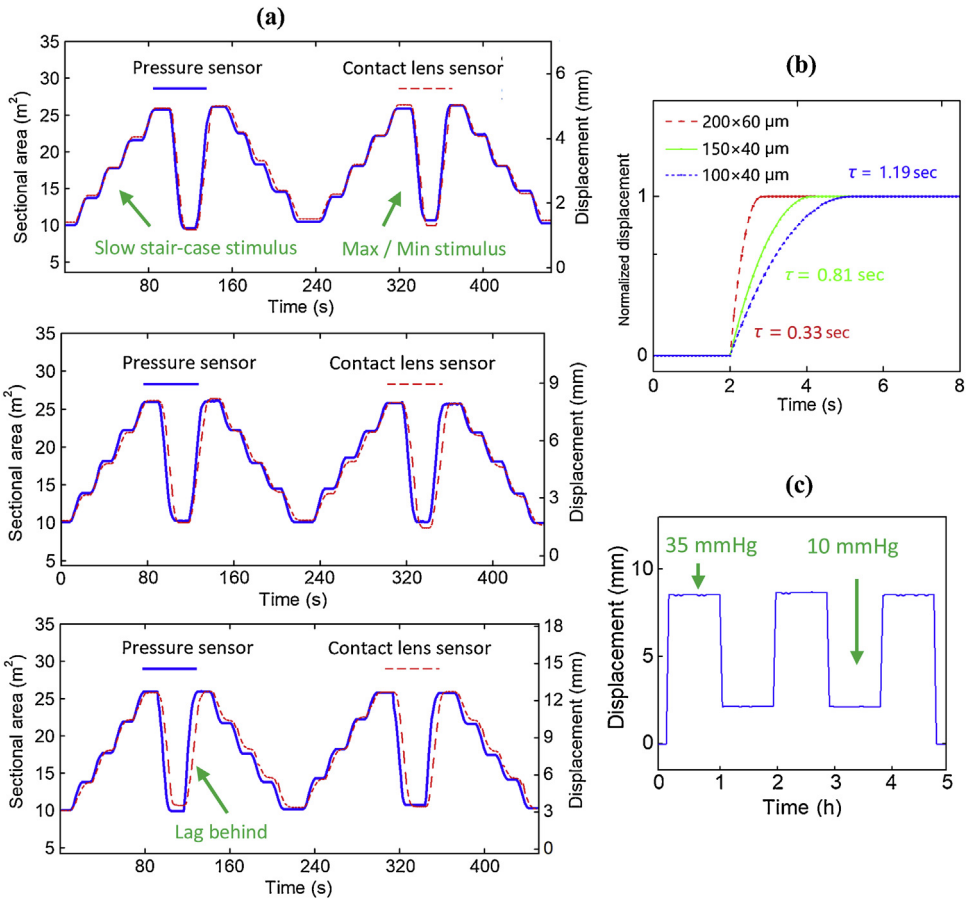

Fig. 6. (a) the displacement response of three devices with different sensing channels (with size of 200 × 60 μm, 150 × 40 μm and 100 × 40 μm, from top to bottom) to the repetitive loads. (b) The displacement change showing the time constant of the three sensors. (b) Long-term stability test.

the porcine eye *ex vivo* for continuous IOP sensing. The porcine eye was fresh enucleated, in particular, the central area of the porcine eye cornea was approximately spherical (with curvature radius of approximately 7.95 mm) while its outer side tended to be flat, the contact lens with the original diameter of 14.4 mm could not be fitted. Therefore, we cut the contact lens smaller (with diameter of 10 mm) and, take the devices with a sensing chamber of 5 mm in diameter and a sensing channel of 150 × 40 μm in size to conduct the experience. In addition, the T-shaped fluidic connector was also used to connect with the pressurization system and the digital pressure sensor respectively, while the remaining interface of the connector was linked with a needle (24 G). The needle was insert into the porcine eye so as to load pressure on the eye wall.

Fig. 7(a) shows the microfluidic contact lens attaching to the porcine eye surface to detect the cornea deformation which was varied with IOP. Fig. 7(b) shows three cycles of increasing and decreasing pressure between 8 and 32 mmHg during the pressurization experiments, in which, the slow stair-case stimulus was used to load pressure on the devices. The blue line represents the IOP, while the red line represents the displacement of the liquid interface. The dynamic demonstrates that the proposed microfluidic contact lens sensor can successfully transfer the deformation of the porcine eye *ex vivo* to the liquid interface displacement (see the Movie.S3). Fig. 7(c) shows the variation of output displacement to the input IOP, the red points and blue points represent the displacement response to different input pressure in increasing and decreasing steps, respectively, while the black line represents the trend line of the sensor response. The microfluidic sensor showed a positive displacement changes and varied linearly with the pressure (with $R^2 = 0.9693$). The sensitivity of device on porcine eye for IOP sensing is 0.2832 mm/mmHg and is lower than that on the silicone rubber model eye. This might be caused by that, the diameter of the device for test was smaller or the mechanical properties of the pig eye was higher than that of the model eye. In addition, the displacement repeated similarly with the same input pressure in different cycles of increasing and decreasing steps, indicating that the microfluidic sensor has a good reproducibility and has a stable trend in stability when the input pressure changes.

3.5. Discussions

Table 3 shows the comparisons results of this study among the related contact lens sensors for IOP sensing with different designs. This study and John's study [40] show the same target of unpowered, continuous and non-invasive IOP sensing by using the contact lens integrated with microfluidic sensor. The major difference is that we use the thermoplastics—PET to manufacture the contact lens. This enables us to thermoform the devices at the lower temperature, 170 °C for 35 s, so as to not affect the characteristics of PDMS. While, their devices can only be prepared at high temperature (300 °C for 5 min), resulting their devices to age yellow [49] and become unwearable for eyes [48]. Moreover, the hard property of the PET reference layer can ensure the devices more stable, especially for long term-monitoring on the living body, compared with these related contact lens sensors [30,34,40]. Since it is more resistant to the circadian interference, such as blinking [50]. In

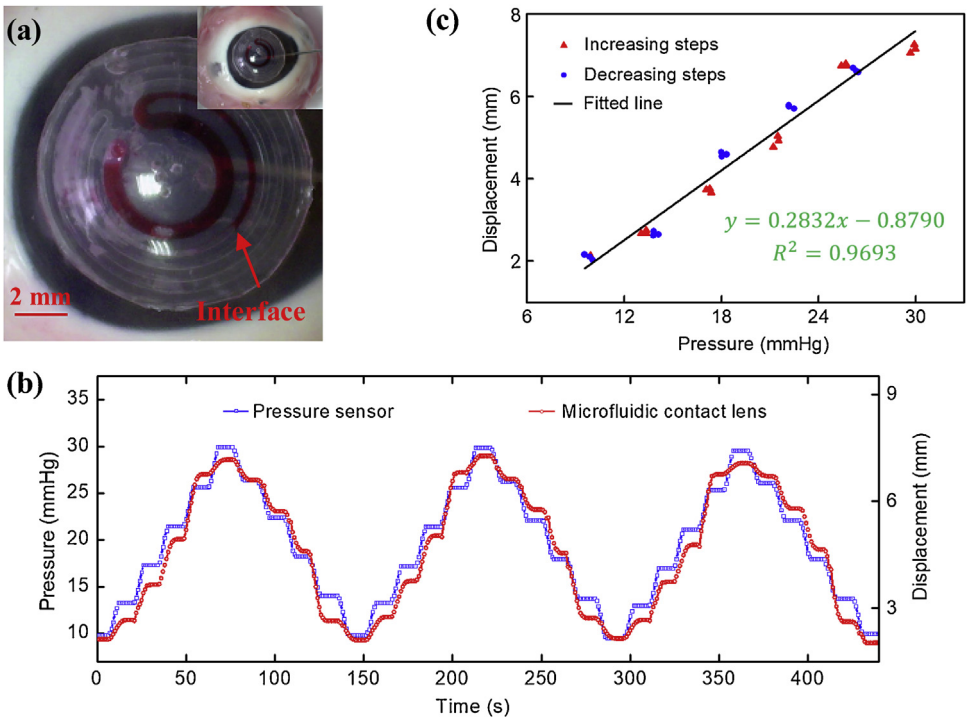

Fig. 7. (a) Picture of the microfluidic contact lens wearing on the porcine eye *ex vivo*; (b) Variation of displacement and IOP during three cycle increasing and decreasing pressure. (c) The displacement response of the devices on porcine eye.

Table 3
Comparison results of this study with the related contact lens sensors for IOP sensing.

	This study	[30]	[34]	[40]
Method	Unpowered and noninvasive	Noninvasive	Noninvasive	Unpowered and noninvasive
Material	PET and PDMS	PDMS	Silicone rubber	Full-PDMS
Manufacture	Thermoforming (170 °C for 35 s)	Integrating	Integrating	Thermoforming (300 °C for 5 min)
Wearability	wearable	wearable	wearable	unwearable
Sensor type	Liquid-displacement	Resistive	Capacitive	Liquid-displacement
Pressure Sensitivity (dynamic range)	Maximum: 0.708 mm/mmHg (0~40 mmHg)	113 μV/mmHg (11-30 mmHg)	23 KHz/mmHg (0-45 mmHg)	0.6 mm/mmHg (0~10 mmHg); 0.13 mm/mmHg (0~46 mmHg)

addition, Table 3 also shows that the proposed IOP sensor can provide higher sensitivity (0.708 mm/mmHg) and large working range (0–40 mmHg) at the same time, this ensures the devices with greater serviceability.

Furthermore, to meet the requirements of future point-of-care glaucoma diagnosis, our microfluidic contact lens could be improved from fabrication. First, the PET film with thinner thickness could be used and the PDMS sensing film could be processed thinner, to reduce the thickness of microfluidic lenses. So, better comfort could be improved and ensures our devices with long-term wearability on human eyes. Moreover, the red dye of functional liquid could be replaced by others, such as sodium fluorescein (a main ingredient of an eye-drop to check the corneal abrasions). Hence, the functional liquid could be ensured with better biocompatibility for eyes, despite its hardly possible to leak out through the out-flow chamber.

4. Conclusions

We have presented the microfluidic contact lens sensors that could provide unpowered, continuous and non-invasive IOP monitoring. The sensing principle is based on that, the deformation of the sensing chamber under pressure would cause the visible movement of the dyed liquid. The theoretical model has been proposed and the FEM simulation was conducted to explore the sensing mechanism and sensing sensitivity under different design parameters (the positions of the sensing chamber and the dimensions of the sensing channel). The characteristics of these sensors are experimental investigated. The results indicate that, for the groups of the inner distributed chamber (with diameters of 5.0 mm or 8.5 mm), the chamber volume decreased with the IOP rising and caused the liquid moving from the chamber to sensing channel; also, their displacements are linearly corresponded to the IOP. For the group of the outer distributed chamber, the chamber volume increase with the IOP rising and the liquid movement is opposite; meanwhile, its displacement response is non-linear. The tests indicate that the sensing sensitivity decreased with the sizes of the sensing channel increase, and the maximum sensitivity could be achieved to 0.708 mm/mmHg in a working range of 0–40 mmHg (with the sensing chamber of 8.5 mm in diameter and the sensing channel of 100 × 40 um in size). Also, cyclical tests were conducted and indicated that the devices had a good reversibility and Long-term stability. Moreover, the device (with the sensing chamber of 5.0 mm in diameter and the sensing channel of 150 × 40 um in size) was test on the porcine eyes *ex vivo*, showing a sensitivity of 0.2832 mm/mmHg in a range of 8–32 mmHg and, the device had a good reproducibility. This work provides a promising approach for unpowered, continuous and non-invasive IOP monitoring.

Acknowledgements

This research is financially supported by National Natural Science Foundation of China (NO. 51375198 and NO. 81471744) and the China Scholarship Council (NO. 201806165005). The authors would thank the WuHan National Research Center for Optoelectronic and the Flexible Electronics Center of HUST for providing the process equipments to manufacture the devices.

Appendix A. Supplementary data

Supplementary material related to this article can be found, in the online version, at doi:https://doi.org/10.1016/j.sna.2019.04.050.

References

[1] H.A. Quigley, et al., Chronic experimental glaucoma in primates. II. Effect of extended intraocular pressure elevation on optic nerve head and axonal transport, Invest. Ophthalmol. Vis. Sci. 19 (1980) 137–152.
[2] B. Bengtsson, et al., Fluctuation of intraocular pressure and glaucoma progression in the early manifest glaucoma trial, Ophthalmology 114 (2007) 205–209.
[3] De Moraes, et al., Risk factors for visual field progression in treated glaucoma, Arch. Ophthalmol. 129 (2011) 562–568.
[4] A. Heijl, et al., Reduction of intraocular pressure and glaucoma progression: results from the Early Manifest Glaucoma trial, Arch. Ophthalmol. 120 (2002) 1268–1279.
[5] H.A. Quigley, et al., The number of people with glaucoma worldwide in 2010 and 2020, Br. J. Ophthalmol. 90 (2006) 262–267.
[6] Y.C. Tham, et al., Global prevalence of glaucoma and projections of glaucoma burden through 2040: a systematic review and meta-analysis, Ophthalmology 121 (2014) 2081–2090.
[7] A.T. Broman, et al., Estimating the rate of progressive visual field damage in these with open-angle glaucoma, from cross-sectional data, Invest. Ophthalmol. Vis. Sci. 49 (2008) 66–76.
[8] E. Hughes, et al., 24-hour monitoring of intraocular pressure in glaucoma management: a retrospective review, J. Glaucoma 12 (2003) 232–236.
[9] M. Detry, et al., Simultaneous 24-hour monitoring of intraocular pressure and arterial blood pressure in patients with progressive and non-progressive primary open-angle glaucoma, Eur. J. Ophthalmol. 6 (1996) 273–278.
[10] J.B. Jonas, et al., Single intraocular pressure measurements and diurnal intraocular pressure profiles, Am. J. Ophthalmol. 139 (2005) 1136–1137.
[11] H. Goldmann, et al., Über applanationstonometrie, Ophthalmologica 134 (1957) 221–242.
[12] K. Mansouri, et al., Meeting an unmet need in glaucoma: continuous 24-h monitoring of intraocular pressure, Expert Rev. Med. Devices 9 (2012) 225–231.
[13] P.J. Chen, et al., Microfabricated implantable parylene-based wireless passive intraocular pressure sensors, J. Microelectromech. Syst. 17 (2008) 1342–1351.
[14] U. Schnakenberg, et al., Initial investigations on systems for measuring intraocular pressure, Sens. Actuators A Phys. 85 (2000) 287–291.
[15] Ç. Varel, et al., A wireless intraocular pressure monitoring device with a solder-filled microchannel antenna, J. Micromech. Microeng. 24 (2014) 45012–45019.
[16] N. Xue, et al., A su-8-based microfabricated implantable inductively coupled passive RF wireless intraocular pressure sensor, J. Microelectromech. Syst. 21 (2012) 1338–1346.
[17] K.S. Shin, et al., Development of novel implantable intraocular pressure sensors to enhance the performance in vivo tests, J. Microelectromech. Syst. 24 (2015) 1896–1905.
[18] A. Donida, et al., A circadian and cardiac intraocular pressure sensor for smart implantable lens, IEEE Trans. Biomed. Circuits Syst. 9 (2016) 777–789.
[19] I.E. Araci, et al., An implantable microfluidic device for self-monitoring of intraocular pressure, Nat. Med. 20 (2014) 1074–1078.
[20] J.O. Lee, et al., A microscale optical implant for continuous in vivo monitoring of intraocular pressure, Microsyst. Nanoeng. 3 (2017) 17057.
[21] N.M. Farandos, A.K. Yetisen, M.J. Monteiro, C.R. Lowe, S.H. Yun, Contact lens sensors in ocular diagnostics, Adv. Healthc. Mater. 4 (2015) 792–810.
[22] A. Vásquez Quintero, et al., Stretchable electronic platform for soft and smart contact lens applications, Adv. Mater. Technol. 2 (2017), 1700073.
[23] J. Kim, et al., Wearable smart sensor systems integrated on soft contact lenses for wireless ocular diagnostics, Nat. Commun. 8 (2017) 14997.
[24] J. Park, et al., Soft, smart contact lenses with integrations of wireless circuits, glucose sensors, and displays, Sci. Adv. 4 (2018), eaap9841.
[25] M. Elsherif, M.U. HASSAN, A.K. Yetisen, H. Butt, Wearable contact Lens biosensors for continuous glucose monitoring using smartphones, ACS Nano 12 (2018) 5452–5462.
[26] H. Yao, et al., A contact lens with integrated telecommunication circuit and sensors for wireless and continuous tear glucose monitoring, J. Micromech. Microeng. 22 (2012), 075007.
[27] A.R. Badawy, M.U. Hassan, M. Elsherif, Z. Ahmed, A.K. Yetisen, H. Butt, Contact lenses for color blindness, Adv. Healthc. Mater. 7 (2018), 1800152.
[28] L. Xinming, et al., Polymeric hydrogels for novel contact lens-based ophthalmic drug delivery systems: a review, Contact Lens Anterior Eye 31 (2008) 57–64.
[29] M. Leonardi, et al., First steps toward noninvasive intraocular pressure monitoring with a sensing contact lens, Invest. Ophthalmol. Vis. Sci. 45 (2004) 3113–3117.
[30] M. Leonardi, et al., Wireless contact lens sensor for intraocular pressure monitoring: assessment on enucleated pig eyes, Acta Ophthalmol. 87 (2009) 433–437.
[31] R. Hubanova, et al., Effect of overnight wear of the Triggerfish® sensor on corneal thickness measured by Visante® anterior segment optical coherence tomography, Acta Ophthalmol. 92 (2014) e119–e123.
[32] V. Laukhin, et al., Non-invasive intraocular pressure monitoring with a contact lens engineered with a nanostructured polymeric sensing film, Sens. Actuators A Phys. 170 (2011) 36–43.
[33] J.C. Chiou, et al., A capacitor-based sensor and a contact lens sensing system for intraocular pressure monitoring, J. Micromech. Microeng. 26 (2015), 015001.
[34] G.Z. Chen, et al., Capacitive contact lens sensor for continuous non-invasive intraocular pressure monitoring, Sens. Actuators A Phys. 203 (2013) 112–118.
[35] G.Z. Chen, et al., Soft wearable contact lens sensor for continuous intraocular pressure monitoring, Med. Eng. Phys. 36 (2014) 1134–1139.
[36] J.C. Yeo, K. Kenry, C.T. Lim, Emergence of the microfluidic wearable technologies, Lab Chip 16 (2016) 4082–4090.
[37] W. Gao, et al., Fully integrated wearable sensor arrays for multiplexed in situ perspiration analysis, Nature 529 (2016) 509–514.
[38] A. Koh, et al., A soft, wearable microfluidic device for the capture, storage, and colorimetric sensing of sweat, Sci. Transl. Med. 8 (2016), 366ra165-366ra165.
[39] N. Jiang, Y. Montelongo, H. Butt, A.K. Yetisen, Microfluidic contact lenses, Small 14 (2018), 1704363.
[40] J. Yan, An unpowered, wireless contact lens pressure sensor for point-of-care glaucoma diagnosis, in: Engineering in Medicine and Biology Society, EMBC, 2011Annual International Conference of the IEEE, 2011, pp. 2522–2525.
[41] R.D.P. Wong, et al., Flexible microfluidic normal force sensor skin for tactile feedback, Sens. Actuators A Phys. 179 (2012) 62–69.
[42] J. Yin, et al., Bioinspired flexible microfluidic shear force sensor skin, Sens. Actuators A Phys. 264 (2017) 289–297.
[43] B. Nie, et al., Microfluidic tactile sensors for three-dimensional contact force measurements, Lab Chip 14 (2014) 4344–4353.
[44] B. Nie, et al., Iontronic microdroplet array for flexible ultrasensitive tactile sensing, Lab Chip 14 (2014) 1107–1116.
[45] S. Agaoglu, et al., Ultra-sensitive microfluidic wearable strain sensor for intraocular pressure monitoring, Lab Chip 18 (2018) 3471–3483.
[46] S.H. Jeong, S. Zhang, K. Hjort, J. Hilborn, Z. Wu, PDMS-based elastomer tuned Soft, stretchable, and sticky for epidermal electronics, Adv. Mater. 28 (2016) 5830–5836.
[47] W. Xi, et al., Ultrathin and wearable microtubular epidermal sensor for real-time physiological pulse monitoring, Adv. Mater. Technol. 2 (2017), 1700016.
[48] H. An, et al., A method of manufacturing microfluidic contact lenses by using irreversible bonding and thermoforming, J. Micromech. Microeng. 28 (2018), 105008.
[49] M. Liu, J. Sun, Q. Chen, Influences of heating temperature on mechanical properties of polydimethylsiloxane, Sens. Actuators A Phys. 151 (2009) 42–45.
[50] G. Christophe, et al., Automated detection and quantification of circadian eye blinks using a contact lens sensor, Transl. Vis. Sci. Technol. 4 (2015) (2015) 4.

Biographies

Hong-Bin An received his B.S. degree in Mechanical engineering from Wuhan University of Technology, China, in 2015. He is currently pursuing the Ph.D. degree in the School of Mechanical Science and Engineering, Huazhong University of Science and Technology, china. His current researches interested are focused on design and development of wearable microfluidics for biomedical applications.

Liang-Zhou Chen is an associate professor of School of Mechanical Science & Engineering of Huazhong University of Science and Technology (HUST). He received his PhD degree in precision instruments and machinery from Shanghai Jiaotong University (SJTU) in 2006, and his M.S. degree and B.S. degree in Measurement technology and instruments from HUST in 1998 and 2001 respectively. His research focuses on precision machinery and optical sensors. He is responsible to several scientific projects, such as National Special Science Instrument Program of China, Special Marine Engineering Equipment Project of National development and reform commission (NDRC) of China, National Natural Science Fund Project of China and other research projects funded by government and enterprises.

Xiao-Jun Liu received his PhD degree in Hong Kong University of Science and Technology, Hong Kong in 2003. He is currently a Professor in School of Mechanical Science & Engineering of HUST and, is conducting research in Optical precision measurement technology and Nanomaterial performance testing.

Bin Zhao is currently a Professor in the School of Mechanical Science & Engineering of HUST, china. He is conducting research in Photoelectric detection technology.

Hong zhang received her PhD degree in Ophthalmology from the Heidelberg University, Germany, in 1989. Currently, she is a Professor in the Tongji Media college of HUST. She has conducted researches in the Clinical diagnosis and treatment of Ophthalmological diseases for many years. Her current researches interested are development of IOP monitor.

Zhi-Gang Wu received his PhD degree in microfluidics from Nanyang Technological University (NTU), Singapore in 2005. Currently, he is a Professor in the School of Mechanical Science & Engineering of HUST, china. He is leading a research group and conducting research in soft robots and, wearable technologies for point-of-care of healthcare and motion monitoring.